

Lipid rafts and the local density of ErbB proteins influence the biological role of homo- and heteroassociations of ErbB2

Peter Nagy^{1,2,3}, György Vereb¹, Zsolt Sebestyén¹, Gábor Horváth¹, Stephen J. Lockett^{4,*}, Sándor Damjanovich^{1,2}, John W. Park⁵, Thomas M. Jovin³ and János Szöllősi^{1,‡}

¹Department of Biophysics and Cell Biology, Medical and Health Science Center and ²Cell-biophysical Workgroup of the Hungarian Academy of Sciences, University of Debrecen, POB 39, Debrecen H-4012, Hungary

³Department of Molecular Biology, Max Planck Institute for Biophysical Chemistry, Am Fassberg 11, Göttingen D-37077, Germany

⁴Bioimaging Group, Life Sciences Division, Lawrence Berkeley National Laboratory, 1 Cyclotron Road, Berkeley, CA 94720, USA

⁵Department of Medicine, Division of Hematology/Oncology, University of California at San Francisco, San Francisco, CA 94143, USA

*Present address: NCI-FCRDC, Boyle Street, Frederick, MD 21702, USA

‡Author for correspondence (e-mail: szollo@jaguar.dote.hu)

Accepted 6 August 2002

Journal of Cell Science 115, 4251-4262 © 2002 The Company of Biologists Ltd

doi:10.1242/jcs.00118

Summary

The ErbB family of transmembrane receptor tyrosine kinases plays an important role in the pathogenesis of many cancers. The four members of the family, ErbB1-4, form various homo- and heterodimers during the course of signal transduction. A second hierarchical level of molecular associations involving 10^2 - 10^3 molecules, termed large-scale clustering, has also been identified, but the regulatory factors and biological consequences of such structures have not been systematically evaluated. In this report, we describe the states of association of ErbB2 and their relationship to local ErbB3 density and lipid rafts based on quantitative fluorescence microscopy of SKBR-3 breast cancer cells. Clusters of ErbB2 colocalized with lipid rafts identified by the GM1-binding B subunit of cholera toxin. Pixel-by-pixel analysis of fluorescence resonance energy transfer between labeled antibodies indicated that the homoassociation (homodimerization) of ErbB2 was proportional to the local density of ErbB2 and inversely proportional to that of ErbB3 and of the raft-specific lipid

GM1. Crosslinking lipid rafts with the B subunit of cholera toxin caused dissociation of the rafts and ErbB2 clusters, an effect that was independent of the cytoskeletal anchoring of ErbB2. Crosslinking also decreased ErbB2-ErbB3 heteroassociation and the EGF- and heregulin-induced tyrosine phosphorylation of Shc. When cells were treated with the anti-ErbB2 monoclonal antibody 4D5 (parent murine version of Trastuzumab used in the immunotherapy of breast cancer), internalization of the antibody was inhibited by crosslinking of lipid rafts, but the antiproliferative activity of 4D5 was retained and even enhanced. We conclude that local densities of ErbB2 and ErbB3, as well as the lipid environment profoundly influence the association properties and biological function of ErbB2.

Key words: ErbB proteins, Lipid rafts, Breast cancer, Fluorescence resonance energy transfer

Introduction

The type I family of transmembrane receptor tyrosine kinases comprises four members: epidermal growth factor receptor (EGFR or ErbB1), ErbB2 (HER2 or Neu), ErbB3 and ErbB4 (Alroy and Yarden, 1997; Yarden and Sliwkowski, 2001). ErbB proteins engage in an extensive network of homo- and heteroassociations resulting in signal diversification (Tzahar et al., 1996). The relative expression levels of the various receptors and the concentrations of their respective ligands determine the composition of homo- and heterodimers (Pinkas Kramarski et al., 1996; Graus Porta et al., 1997). ErbB2 is the preferred heteroassociation partner of all other ErbB proteins, enhancing ligand binding affinity and signaling potency by virtue of its potent latent kinase activity (Karunakaran et al., 1996). Activation-induced endocytosis and downregulation are important in limiting the duration of receptor activation, but their efficiency is low for all members of the ErbB family with the exception of ErbB1 (Baulida et al., 1996). This is probably

due to impaired coupling of cbl, a protein thought to be involved in activation-induced degradation, to ErbB2, ErbB3 and ErbB4 (Levkowitz et al., 1996). The significance of ErbB2 is underscored by its overexpression in about 30% of breast carcinomas, a phenomenon associated with poor prognosis (Slamon et al., 1987).

The signaling network of ErbB proteins is based on receptor homo- and heterodimers. In addition to these small-scale associations, higher order associations involving large-scale clusters of ErbB2 have also been identified (Nagy et al., 1999b). These clusters contain hundreds of ErbB2, are $\sim 0.5 \mu\text{m}$ in diameter, a size that increases upon ErbB2 activation. The significance of such large-scale protein clusters probably results from the high local concentration of ErbB and other signaling proteins facilitating the formation of receptor complexes (Nagy et al., 1999a).

ErbB2 plays an important role in the development and progression of many breast cancers and other malignancies

(Park et al., 2000). An anti-ErbB2 monoclonal antibody, 4D5, inhibits the proliferation of tumor cells that overexpress ErbB2 (Sarup et al., 1991). The humanized version of 4D5 (Trastuzumab, Herceptin™) has significant anticancer activity (Cobleigh et al., 1999; Slamon et al., 2001). Its exact mechanism of action is as yet unclear. The antibody induces partial tyrosine phosphorylation of ErbB2 but does not activate the MAP kinase pathway, although it does activate the cyclin-dependent kinase inhibitor p27KIP (Sliwkowski et al., 1999). It has been proposed that the antiproliferative activity of Trastuzumab is due largely to the downmodulation of surface ErbB2 by receptor-mediated endocytosis (Sarup et al., 1991; Sliwkowski et al., 1999). Cbl-mediated ubiquitination is thought to play a key role in this process (Klapper et al., 2000; Levkowitz et al., 2000). Antibodies that efficiently internalize ErbB2 but fail to inhibit tumor cell proliferation have also been identified (Neve et al., 2001), suggesting that antibody-mediated internalization may not be a good marker of anti-tumor activity.

Higher order associations (i.e. the organization of individual and oligomeric membrane proteins into several hundred-nanometer-scale complexes) have attracted increased attention in studies of receptor biology and signal transduction. Membrane domains are often thought of as organizing forces beyond such associations. For example, lipid rafts, sphingolipid- and cholesterol-rich membrane microdomains, participate in diverse cellular functions such as membrane trafficking and receptor signaling (Simons and Ikonen, 1997; Janes et al., 1999). There is intense debate about the size and nature of lipid rafts, but recent evidence supports the existence of small (<0.1 µm in diameter) lipid rafts that can dynamically associate with each other to form larger signal transducing platforms (Harder and Simons, 1997; Kurzchalia and Parton, 1999; Pralle et al., 2000; Edidin, 2001; Anderson and Jacobson, 2002). Lipid rafts and a special form thereof, caveolae, are thought to be involved in EGFR-mediated signaling (Furuchi and Anderson, 1998; Mineo et al., 1999) presumably by altering the activity of protein kinases (Ilangumaran et al., 1999) and changing the association state of membrane proteins (Bodnár et al., 1996; Vereb et al., 2000; Matkó et al., 2002).

We have previously reported the existence of plasma membrane domains in which the homoassociation of ErbB2 is unusually high (Nagy et al., 1998). The significance of this finding is underlined by the fact that overexpression-driven constitutive homoassociation of ErbB2 induces ligand-independent activation of ErbB2 and other ErbB proteins (Worthylake et al., 1999). Although the overall effect of changes in the relative expression levels of ErbB proteins has already been studied (Tzahar et al., 1996), the role of local differences in the relative densities of receptors, which may explain differences in the association of proteins within a single cell (Chamberlin and Davies, 1998), has not been previously addressed. In our current experiments we show that membrane domains with high degree of ErbB2 homoassociation have high ErbB2 and low ErbB3 densities. The association state of ErbB2 is also influenced by lipid rafts. ErbB2 is dislodged from the latter after crosslinking GM1, a raft-associated ganglioside (Harder et al., 1998), by the B subunit of cholera toxin (CTX-B), which is associated with decreased ErbB2-ErbB3 heterodimerization and reduced tyrosine phosphorylation of

ErbB2 upon heregulin stimulation. It is of interest to point out that 4D5-mediated internalization of ErbB2 is blocked in CTX-B-pretreated cells, whereas the antiproliferative effect of 4D5 is not. Our results emphasize that alterations in the local environment of ErbB2 strongly influence its association properties with significant consequences for its biological activity.

Materials and Methods

Cells lines

The SKBR-3 breast tumor cell line was obtained from the American Type Culture Collection (Rockville, MD) and grown according to its specifications to confluency. For microscopic experiments cells were cultured in slide chambers (Nunc, Naperville, IL), and labeled and measured without trypsinisation. For flow cytometric measurements cells were harvested with trypsinization.

Antibodies, growth factors

4D5 and 7C2 antibodies against the ErbB2 protein were a kind gift from Genentech (South San Francisco, CA), and were labeled with fluorescent dyes for FRET and for colocalization measurements. The dye/protein ratio was 1-3 as determined by spectrophotometric measurements. The H3.90.6 anti-ErbB3 antibody was purchased from NeoMarkers (Fremont, CA), and the sc-894 polyclonal rabbit antibody against caveolin was from Santa Cruz Biotechnology (Heidelberg, Germany). Cy2-, Cy3- and Cy5-labeled polyclonal rabbit Fab fragments against mouse IgG (anti H+L) were from Jackson Immunoresearch (West Grove, PA). The anti-phosphotyrosine antibody PY99 (sc-7020) and the anti-Shc antibody (sc-967) were from Santa Cruz Biotechnology (Santa Cruz, CA). The anti-ErbB2 antibody c-neu/Ab-3 (OP15) was from Calbiochem (Darmstadt, Germany). Protein G-coated Sepharose 'Fast flow' beads were purchased from Sigma-Aldrich (Schnelldorf, Germany).

Epidermal growth factor and the EGF-like domain of heregulin-β1 were from R&D Systems (Minneapolis, MN). Cells were starved in 0.1% FCS-containing medium for 48 hours before stimulation with EGF or heregulin.

Labeling of cells with antibodies and subunit B of cholera toxin

ErbB proteins were labeled with saturating concentration of antibodies for 30 minutes on ice in PBS. Unbound antibodies were removed by washing twice with PBS. When two primary labeled antibodies were used to label cells, they were added simultaneously. When one of the labelings was indirect, cells were first incubated with the unlabeled primary antibody followed by the dye-conjugated secondary Fab. Subsequently, cells were labeled with a labeled primary antibody against the other antigen.

Prior to labeling caveolin, cells were fixed in 3.7% formaldehyde (30 minutes on ice) and incubated with the sc-894 anti-caveolin antibody in the presence of 0.1% BSA and 0.1% TritonX-100 for 30 minutes on ice followed by secondary labeling with Cy3-conjugated F(ab')₂ fragment of goat anti-rabbit immunoglobulin (Jackson Immunoresearch, West Grove, PA).

In order to label lipid rafts cells were incubated in the presence of 8 µg/ml FITC-labeled subunit B of cholera toxin (Sigma-Aldrich, Schnelldorf, Germany) for 30 minutes on ice. For crosslinking lipid rafts incubation with subunit B of cholera toxin was carried out at 37°C for 30 minutes.

Confocal microscopy

A Zeiss LSM410 confocal laser scanning microscope (Carl Zeiss, Thornwood, New York) was used to image cells. Alexa488, Cy2 and

FITC were excited with the 488 nm line of an argon/krypton ion laser and emission from these fluorophores was detected through an FT 488/568 nm dual-band dichroic mirror and a 515-565 nm band-pass filter. Cy3 was excited with the 568 nm line of an argon/krypton laser and emission was detected through an FT 488/568 nm dual-band dichroic mirror and a 575-640 nm band-pass filter. Cy5 was excited at 647 nm and emission was measured through a FT 665 nm long-pass dichroic mirror.

During the experiments with membrane clusters of ErbB proteins, the focal plane of the confocal microscope was adjusted such that either the top or the bottom flat layer of the cell membrane could be imaged in a single confocal slice.

Donor photobleaching FRET measurements

In some of the experiments, the association of membrane proteins was measured using the donor photobleaching FRET method (Jovin and Arndt Jovin, 1989). Briefly, one of the proteins was labeled with a fluorescein (donor)-labeled antibody and the other protein was labeled with a Cy3 (acceptor)-labeled antibody (double-labeled sample). Another sample was also prepared in which only the donor-labeled antibody was applied (donor only sample). The kinetics of donor photobleaching was measured in both samples. The fluorescence intensity curves were fitted to a double exponential equation with a custom-written program in LabView (National Instruments, Austin, TX). An effective rate constant was calculated by taking the amplitude-weighted time constants of the exponential terms. Any process (e.g. FRET) competing with photobleaching slows the rate of the process. Therefore it is possible to calculate the FRET efficiency on a pixel-by-pixel basis by comparing the rate of donor photobleaching in the double-labeled sample to that in the donor-only-labeled sample according to the expression $FRET = 1 - \tau_{eff,D} / \tau_{eff,DA}$, where $\tau_{eff,D}$ is the average effective photobleaching time constant in the donor-only-labeled sample, and $\tau_{eff,DA}$ is the effective photobleaching time constant of a pixel in the donor-acceptor double-labeled sample.

Acceptor photobleaching FRET measurements

This technique is based on the detection of increased donor fluorescence intensity following irreversible photodestruction of the acceptor (Wouters et al., 1998). A sample was labeled with Cy3- and Cy5-tagged antibodies. First, an image was taken in the Cy3 (donor) channel (I_q) followed by an image in the Cy5 (acceptor) channel. Then, the acceptor was bleached completely, after which another Cy3 image was taken reporting the unquenched fluorescence intensity of the donor (I_{uq}). Images were corrected for spectral spillover, and the second Cy3 image was corrected for bleaching by the 647 nm laser line used to bleach Cy5. The FRET efficiency was calculated according to the equation $FRET = 1 - I_q / I_{uq}$.

Analysis of correlation between FRET efficiency and fluorescence intensity

In order to correlate the FRET efficiency (measured either with the donor or the acceptor photobleaching FRET method) with the fluorescence intensity on a pixel-by-pixel basis, images were analyzed with Scil-Image (University of Amsterdam, The Netherlands) after correction for shift and spectral spillover. The correlation between FRET efficiency and unquenched donor fluorescence intensity was calculated and plotted according to Demandolx and Davoust (Demandolx and Davoust, 1997).

Calculation of the overlap between clusters

Low frequency background was removed using either a Fourier transformation based method (Hwang et al., 1998) or top-hat

transformation (Glasbey and Horgan, 1995). Low frequency background is a constant or a smoothly changing intensity component that may be caused by inhomogeneous illumination, autofluorescence or non-specific staining. Removal of high frequency background (smoothing) was carried out either by low-pass filtering or a morphology operation (opening) (Glasbey and Horgan, 1995). Cluster and background pixels were discriminated with the entropy threshold segmentation algorithm of Scil-Image, and the distribution of particle sizes in this binary mask was determined with ScionImage (Scion Corp., Frederick, MD). Cluster diameter was determined by judiciously positioning the cursor on the screen on opposing edges of the bright regions (Nagy et al., 1999b). In order to calculate the area of overlap between clusters, segmented binary images (in which digit 1 and 0 correspond to cluster and background pixels, respectively) recorded in the different fluorescence channels were multiplied with each other. In the resulting image foreground pixels (value 1) reflect the overlap of clusters in the two input images. The fractional overlap was calculated by dividing the area of foreground pixels in the resulting image by the area of foreground pixels in one of the original images. Since this area was approximately the same in both original images, we report only one of the obtained ratio values.

Flow cytometric energy transfer measurements

A modified Becton Dickinson FACStar Plus flow cytometer equipped with dual argon ion laser excitation was used to measure the FRET efficiency between fluorescently labeled membrane proteins. This parameter is a quantitative measure of protein associations and can be derived from three fluorescence intensities (Szöllösi et al., 1984). Two intensities resulted from excitation at 488 nm and detection at 540 ± 20 and above 580 nm, and the third signal was excited at 514 nm and detected above 580 nm. Forward angle light scattering (at 514 nm) was used to gate out debris. All data were stored in list mode format. FRET efficiency was calculated on a cell-by-cell basis from the three fluorescence intensities of 10,000 cells.

Flow cytometric measurement of antibody internalization

Three methods were used to detect antibody internalization. (1) SKBR3 cells were incubated with unlabeled 4D5 (10 $\mu\text{g/ml}$) at 37°C. Samples were taken every 10 minutes, and non-internalized ErbB2 was labeled with Alexa488-7C2 for 30 minutes on ice. Fluorescence was detected with a FacsCalibur Flow Cytometer. (2) SKBR3 cells were incubated in the presence of 10 $\mu\text{g/ml}$ 4D5 antibody at 37°C. The non-internalized fraction of 4D5 was labeled with Cy2-tagged Fab fragments of anti-mouse IgG, and the fluorescence intensity of Cy2 was measured on the flow cytometer. (3) SKBR3 cells were treated with fluorescein labeled 4D5 antibody at 37°C. Samples taken every 10 minutes were divided into two parts. Part 1 was subjected to acid-wash (pH 2.4, 3 min) in order to remove 4D5 from the cell surface (Baulida and Carpenter, 1997). Part 2 was not acid-treated. The difference between the fluorescence intensities of these two samples represented the amount of 4D5 on the cell surface.

Measurement of cell proliferation

50,000 cells were seeded in a culture dish and kept in the presence of 10% FCS for 1 day. They were subsequently incubated in medium containing 0.1% FCS for 1 day. This was followed by a 5-day culture in the presence of 10% FCS. In order to study the antiproliferative effect of 4D5, 10 $\mu\text{g/ml}$ of the antibody was added to the medium with or without 8 $\mu\text{g/ml}$ cholera toxin (subunit B). The culture medium supplemented with 4D5 (and cholera toxin) was replenished every second day. On day 5 the cells were counted and the cell surface expression of ErbB2 was determined by labeling cells with Alexa488-7C2.

Measurement of tyrosine phosphorylation of ErbB2 and Shc

Cells were scraped off the culture substrate. Whole cell lysates of control or stimulated cells were prepared by incubating the cells in lysis buffer (20 mM Tris-HCl, 150 mM NaCl, 10% (w/v) glycerol, 1 mM EGTA, 1% (w/v) Triton X-100, 1 mM Na_3VO_4 , 1 mM PMSF, Complete Mini protease inhibitor cocktail from Roche, pH 7.5) for 10 minutes on ice. The lysate was centrifuged at 12,000 *g*, and ErbB2 or Shc was immunoprecipitated from the supernatant using OP15 and sc-967 antibodies, respectively, and protein G beads. The immunoprecipitates were run on SDS-polyacrylamide gels, and blotted to nitrocellulose membranes. The membranes were probed with anti-phosphotyrosine antibody PY99, then stripped and reprobed with either anti-ErbB2 or anti-Shc antibodies to check whether equivalent amounts of proteins were immunoprecipitated in each sample. Bands on the blots were quantitated using enhanced chemiluminescence (Amersham, Freiburg, Germany).

Results

ErbB2 homoassociation is not significantly different inside and outside large-scale clusters

Previously we have found that the homoassociation of ErbB2 is uneven on the cell surface, i.e. there are membrane patches with a diameter of ~ 0.5 - $1 \mu\text{m}$ in which ErbB2 homoassociation is significantly higher than in the surrounding area (Nagy et al., 1998). Later we have identified large-scale clusters of ErbB2 containing ~ 1000 ErbB2 proteins in which the density of ErbB2 is 1-2 orders of magnitude higher than outside of them. Their characteristic diameter is $\sim 0.5 \mu\text{m}$ (Fig. 2A) (Nagy et al., 1999b). The similar size of large-scale ErbB2 clusters and membrane patches showing a high degree of ErbB2 homoassociation raised the possibility that the two might be related. Therefore we measured the homoassociation of ErbB2 on a pixel-by-pixel basis using the donor pbFRET technique in confocal microscopy (Jovin and Arndt Jovin, 1989) in order to find out whether ErbB2 homoassociation was the same inside and outside of large-scale clusters of ErbB2. The fluorescence intensity of pixels outside large-scale clusters was not high enough for reliable FRET measurements prompting two approaches for increasing the signal-to-noise ratio. First, large polygon-shaped regions of interest (ROI) were placed separately on areas outside and inside large-scale clusters, and the fluorescence intensity was summed inside these ROIs. The FRET efficiency was calculated on the summed fluorescence intensities. There was no significant difference between the FRET efficiencies evaluated over pixels inside and outside the large-scale clusters. In FRET experiments the FRET efficiency is a measure of protein associations: the higher the FRET efficiency is, the tighter the labeled proteins associate with each other. Therefore, the lack of any significant difference in the measured FRET efficiencies indicated that the homoassociation of ErbB2 was the same inside and outside ErbB2 clusters: FRET efficiencies for ErbB2 homoassociation were $16 \pm 3\%$ and $18 \pm 3\%$ (mean \pm s.e.m.) for pixels inside and outside ErbB2 clusters, respectively. According to the second approach, the size of images was reduced in a way that square-shaped areas (superpixels) consisting of 3×3 , 5×5 or 7×7 pixels were collapsed to a single pixel, the fluorescence intensity of which was the summed intensity of the area it replaced. Evaluation of the FRET efficiency was carried out on a pixel-by-pixel basis on these compressed images, separately for superpixels outside and inside large-scale clusters. These

calculations corroborated that there was no significant difference between the homoassociation of ErbB2 inside and outside large-scale clusters of this protein (FRET efficiencies for ErbB2 homodimerization were $17 \pm 2\%$ and $16 \pm 2\%$ for superpixels inside and outside large-scale ErbB2 clusters, respectively, with all three sizes of superpixels).

ErbB2 homoassociation is influenced by the local density of ErbB2 and ErbB3

Since the homoassociation of ErbB2 did not differ significantly inside and outside large-scale clusters, we turned our attention to the local densities of ErbB2 and ErbB3 as possible determinants of ErbB2 homoassociation. SKBR-3 breast tumor cells were labeled with FITC-4D5 and Cy3-4D5 as donor-acceptor pair against ErbB2, and ErbB3 was labeled indirectly using a Cy5-tagged secondary antibody. The homoassociation of ErbB2 was calculated on a pixel-by-pixel basis using the donor pbFRET technique and plotted as a function of the local ErbB2 and ErbB3 densities. The analysis, carried out on pixels inside ErbB2 clusters, showed that ErbB2 homoassociation was positively correlated with the local density of the protein, but negatively correlated with the local density of ErbB3 (Fig. 1). A very similar dependence of ErbB2 homoassociation on the local densities of ErbB2 and ErbB3 was found outside clusters; i.e. there were areas with high ErbB2 homoassociation outside clusters as well (data not shown). However, the signal-to-noise ratio was much lower in pixels outside clusters, therefore we restricted our detailed analysis to the clusters. Membrane patches with unusually high ErbB2 homoassociation were located in areas where the local density of ErbB2 was high and that of ErbB3 was comparatively low (Fig. 2A-C), as shown in Fig. 2D-F. In addition, for areas with high ErbB2 intensity and very high ErbB3 density (as those

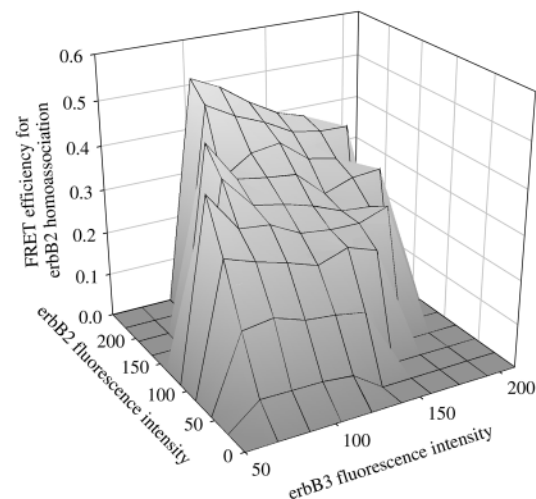


Fig. 1. Dependence of ErbB2 homoassociation on local parameters. SKBR-3 breast tumor cells were labeled with FITC-4D5 and Cy3-4D5 against ErbB2 to measure the homoassociation of ErbB2; ErbB3 was labeled with Cy5-tagged secondary Fab following labeling with H3.90.6. The homoassociation of ErbB2 was measured with the donor pbFRET method, and it was correlated with the local density of ErbB2 and ErbB3 on a pixel-by-pixel basis. The average FRET efficiency for ErbB2 homoassociation is plotted as a function of the local density of ErbB2 and ErbB3.

marked with arrows in images A-C, Fig. 2), the homoassociation of ErbB2 is lower than would be expected from the high ErbB2 density alone.

ErbB2 clusters colocalize with lipid rafts

Lipid rafts and lipid raft clusters are envisioned to be in the range of ~10-1000 nm in size (Harder et al., 1998; Jacobson and Dietrich, 1999; Anderson and Jacobson, 2002). Since lipid rafts can serve as signal transduction platforms (Kurzchalia and Parton, 1999), determining the colocalization between ErbB2 and lipid rafts is important and relevant. Lipid rafts were visualized by labeling cells with FITC-labeled subunit B of cholera toxin (CTX-B), which binds GM1 ganglioside, a lipid component highly abundant in lipid rafts (Harder et al., 1998). ErbB2 was labeled with Cy3-4D5. These experiments revealed that the overlap between lipid rafts and ErbB2 clusters was $77\pm6\%$ (Fig. 3A).

ErbB2 homoassociation is negatively correlated with the density of GM1

We next examined the spatial relationship between lipid rafts and the homoassociation of ErbB2. Rafts were labeled with FITC-CTX-B, and ErbB2 was labeled with a 1:1 mixture of Cy3- and Cy5-tagged 4D5. ErbB2 homoassociation was measured with the acceptor photobleaching technique. We found a negative correlation between ErbB2 homoassociation and the fluorescence intensity of FITC-CTX-B (Fig. 3A,B, Fig. 4). We detected no FRET between FITC-CTX-B and Cy3-4D5 (data not shown) implying that the fluorescence intensity of FITC-CTX-B reflected its local density. As CTX-B labels GM1 ganglioside, an abundant lipid component of lipid rafts, we concluded that there was a negative correlation between ErbB2 homoassociation and the local density of the raft marker.

Cells were stimulated with EGF (50 ng/ml), heregulin (50 ng/ml) or MAB 4D5 (10 μ g/ml) to determine whether the colocalization between rafts and large-scale clusters of ErbB2 was altered upon activation. The colocalization of ErbB2 clusters and lipid rafts was not significantly influenced by any of the above treatments, as evidenced by similar cluster overlap values ($77\pm6\%$ on control cells; $71\pm6\%$, $76\pm9\%$ and $73\pm9\%$ after stimulation with EGF, heregulin and 4D5, respectively). We have previously reported that the size of large-scale ErbB2 clusters increases upon stimulation of cells with EGF, heregulin or 4D5 (Nagy et al., 1999b). Thus, the fact that the overlap between large-scale ErbB2 clusters and lipid rafts did not change upon any of these

stimuli, suggested that the size of lipid rafts also increased after stimulation with EGF, heregulin or 4D5. This conclusion was confirmed by calculation of lipid raft diameter, which increased from 0.43 ± 0.02 μ m in control cells to 0.53 ± 0.02 μ m, 0.54 ± 0.03 μ m and 0.51 ± 0.03 μ m upon stimulation with EGF, heregulin and 4D5, respectively ($P<0.05$ for the increase; Fig. 3C). Since both the control and the treated samples were labeled with FITC-CTX-B and labeling was carried out on ice, we believe that the observed increase in raft size was not due to pentavalent binding of FITC-CTX-B.

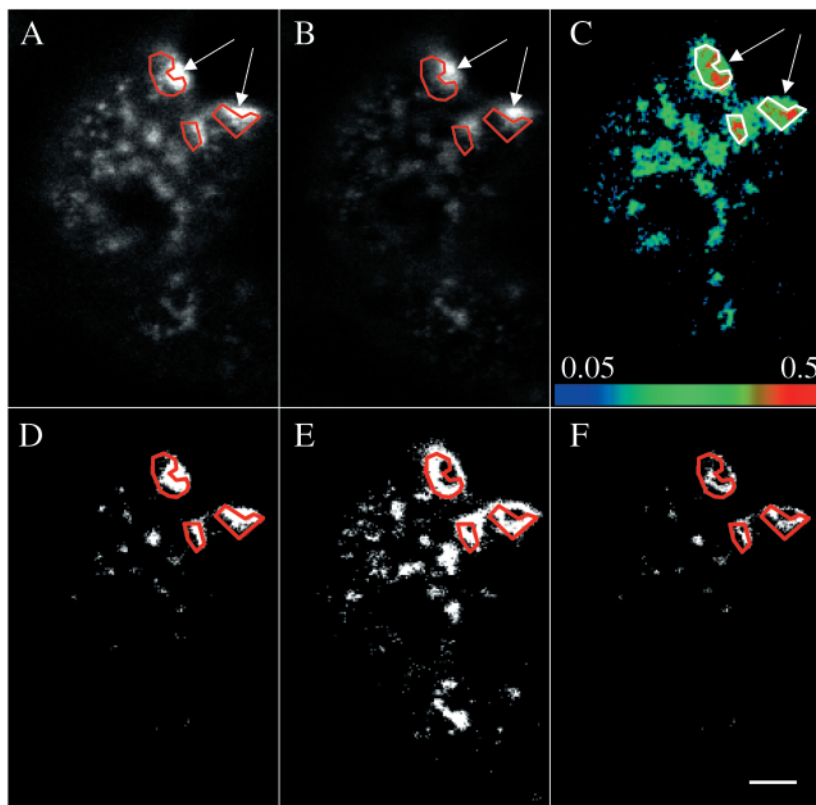


Fig. 2. Membrane areas with anomalously high ErbB2 homoassociation colocalize with membrane domains with high ErbB2 and comparatively low ErbB3 densities. SKBR-3 breast tumor cells were labeled with FITC-4D5 and Cy3-4D5 against ErbB2, and with unlabeled H3.90.6 anti-ErbB3 antibody followed by secondary labeling with a Cy5-tagged Fab. Images A and B show the fluorescence intensity distribution of Cy3-4D5 (ErbB2) and the Cy5-tagged secondary Fab (ErbB3), respectively. The FRET efficiency for ErbB2 homoassociation is displayed in image C. The areas inside the white polygons in image C have the highest FRET values. The same areas are marked with red polygons in images A, B, D-F. These areas have very high ErbB2 density and comparatively low ErbB3 density. The areas at the head of the arrows have the highest ErbB2 and ErbB3 densities, but ErbB2 homoassociation in these pixels is lower than inside the marked areas. Image A was thresholded, and pixels with high ErbB2 fluorescence intensity are white in image D, whereas pixels with intensity below the threshold are black. Image B was 'bi-thresholded': two intensity values were determined, and only pixels whose intensity is between the two threshold values are white in image E, all other pixels are displayed in black. Threshold values were adjusted so that white pixels in image E have low ErbB3 intensities, but still above a certain level. Pixels with intensity values lower than the lower threshold are background pixels, and they have to be excluded from the analysis. In image F a pixel is displayed in white if the pixel is white in both image D and E. The distributions of white areas in image F correlate with pixels with high ErbB2 homoassociation in image C. Bar, 1 μ m.

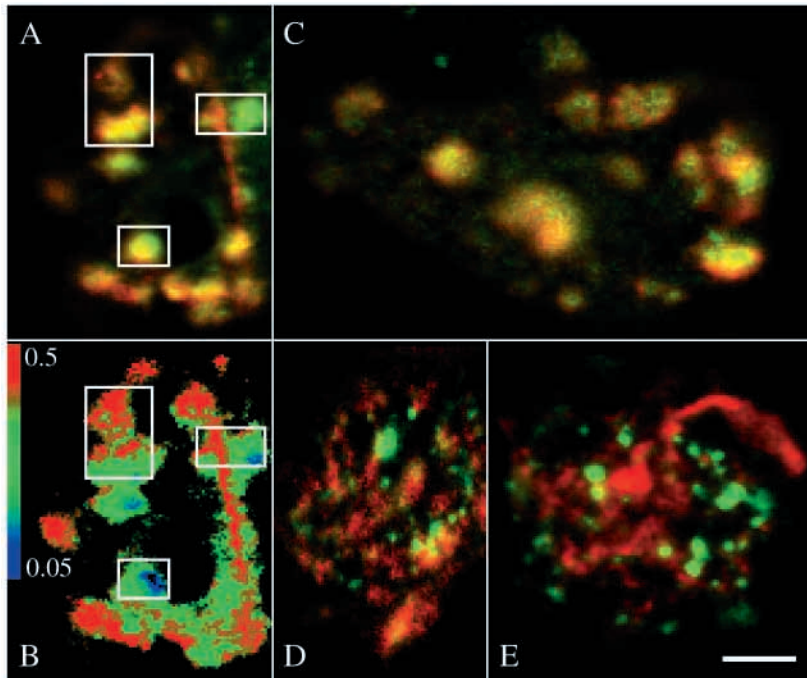


Fig. 3. The relationship between lipid rafts and the small- and large-scale clustering of ErbB2. (A,B) SKBR-3 cells were labeled with FITC-CTX-B, Cy3-4D5 and Cy5-4D5 Fab. The FITC (green) and Cy3 (red) channels are overlaid in image A. Yellow areas correspond to colocalization between CTX-B-labeled lipid rafts and ErbB2 clusters. The homoassociation of ErbB2 was calculated using the acceptor photobleaching FRET method, and the FRET efficiency is displayed in panel B. FRET efficiency is color-coded according to the color-scale. The white boxes mark areas with inverse correlation between the local CTX-B-labeling density and ErbB2 homoassociation: the greener the area is in image A, the lower the FRET efficiency is in the corresponding part of the cell in image B. (C) Heregulin-stimulated SKBR-3 cells were labeled with FITC-CTX-B and Cy3-4D5 Fab. (D) SKBR-3 cells were treated with FITC-CTX-B at 37°C for 30 minutes, and they were subsequently labeled with Cy3-4D5 Fab. (E) SKBR-3 cells were pretreated with FITC-CTX-B and then incubated with Cy3-4D5 antibody at 37°C for 30 minutes. In part A, C and E the FITC image (green) is overlaid on the Cy3 (red) image. Yellow areas correspond to significant colocalization between lipid rafts and ErbB2 clusters. Bar, 1 µm.

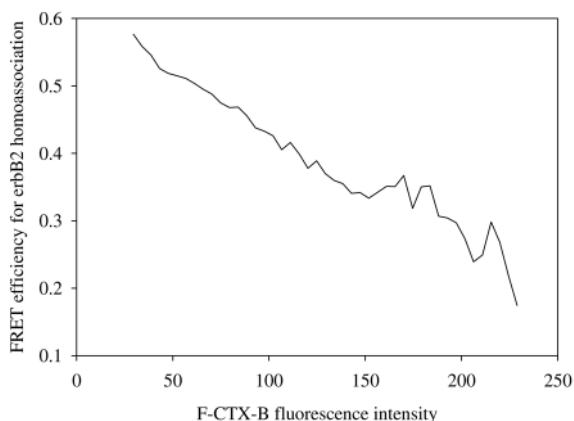


Fig. 4. Lipid rafts influence the homoassociation of ErbB2. Lipid rafts were visualized with FITC-CTX-B, and ErbB2 was labeled with Cy3-4D5 and Cy5-4D5 antibodies in order to measure its homoassociation with the acceptor photobleaching FRET method. FRET efficiency was averaged in pixels with the same FITC-CTX fluorescence intensity, and the average FRET efficiency is plotted as a function of lipid raft labeling.

CTX-B induces significant changes in the large-scale association of ErbB2

In view of the inverse correlation between the density of GM1 ganglioside and ErbB2 homoassociation, we investigated whether lipid raft crosslinking by CTX-B had any effect on the association of ErbB2. CTX-B not only binds GM1, but prolonged exposure of cells to CTX-B at 37°C can crosslink lipid rafts and induce characteristic changes in the distribution of membrane proteins (Harder et al., 1998). Cells were first treated with 8 µg/ml FITC-CTX-B at 37°C for 30 minutes, and then labeled with Cy3-4D5 Fab against ErbB2 on ice. Analysis by confocal microscopy showed that the overlap

between lipid rafts and large-scale clusters of ErbB2 significantly ($P < 0.05$) decreased to $29 \pm 9\%$ (Fig. 3D), implying that crosslinking of GM1 by CTX-B sequestered these domains from ErbB2. By crosslinking GM1 CTX-B induces translational diffusion of lipid rafts and the accumulation of GM1 at sites of endocytosis (Nichols, 2002). One possibility is that cytoskeletal anchoring of ErbB2 might impede its movement with lipid rafts, resulting in ErbB2 being left behind. However, disrupting microfilaments with cytochalasin D treatment (10 µg/ml, 2.5 hours, 37°C) did not perceptibly modify the CTX-B-induced separation between lipid rafts and large-scale clusters of ErbB2; the overlap between lipid rafts and large-scale clusters of ErbB2 was $28 \pm 5\%$ in CTX- and cytochalasin D-treated cells. Cytochalasin D by itself did not change the colocalization between ErbB2 clusters and lipid rafts, from which we conclude that cytoskeletal anchoring was not responsible for the inability of ErbB2 to move with lipid rafts.

Relationship between ErbB2 and caveolin clusters to GM1-enriched domains

Caveolae are considered to be specialized lipid rafts, that can be visualized with confocal microscopy (Kurzchalia and Parton, 1999). In order to determine whether FITC-CTX-B-labeled domains correspond to caveolae, we labeled SKBR-3 cells with an anti-caveolin antibody and FITC-CTX-B (Fig. 5A). There was an almost complete separation between caveolae and the domains labeled by CTX-B as evidenced by the low cluster overlap value ($13 \pm 4\%$). This result suggested that ErbB2 protein clusters, which colocalize with CTX-B, should not overlap with caveolae. Indeed, we found only a negligible colocalization between ErbB2 clusters and caveolae ($17 \pm 6\%$, Fig. 5B). However, CTX-B induced crosslinking of GM1 induced its migration into caveolae, leaving ErbB2 clusters behind (Fig. 5C).

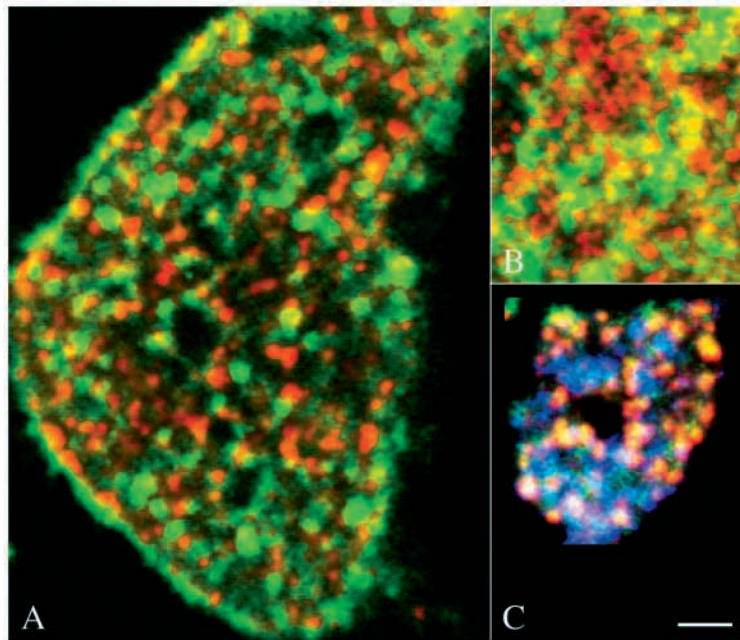


Fig. 5. Relationship between caveolin, GM1-enriched domains and ErbB2 clusters. (A) Quiescent SKBR-3 cells were labeled with FITC-CTX-B (green channel) and with anti-caveolin antibody sc-894 followed by secondary staining with Cy3-conjugated goat anti-rabbit immunoglobulin to visualize sc-894 labeling (red channel). (B) Quiescent SKBR-3 cells were stained against ErbB2 (with Alexa488-4D5, green channel) and against caveolin (as in part A, red channel). (C) SKBR-3 cells were treated with FITC-CTX-B for 30 minutes at 37°C (green channel), and then stained against ErbB2 (Cy5-4D5, blue channel) and against caveolin (as in part A, red channel). Bar, 1 μ m.

CTX-B-induced changes in the small-scale association of ErbB2

We investigated the small-scale association of ErbB2 in control and CTX-B-treated cells using flow cytometric FRET measurements. In these experiments, cells were treated with unlabeled CTX-B, and then labeled with donor- and acceptor-labeled antibodies against the ErbB proteins. The heteroassociation of ErbB2 with ErbB3 significantly decreased, but the homoassociation of ErbB2, and its heteroassociation with ErbB1 was not affected by CTX-B treatment (Fig. 6A). In control experiments, CTX-B treatment did not change the expression level of ErbB1, ErbB2 and ErbB3 implying that the measured changes in the FRET efficiencies reflect alterations in protein association. One possible origin for the decreased heteroassociation between ErbB2 and ErbB3 is that CTX treatment separates ErbB2 but not ErbB3 from lipid rafts. This would result in the separation of large-scale clusters of ErbB2 and ErbB3, which would make their heteroassociation impossible. However, confocal microscopy showed that both ErbB2 and ErbB3 remained in the same large-scale clusters after CTX treatment (data not shown).

ErbB2 and Shc tyrosine phosphorylation induced by EGF and heregulin in cells pretreated with CTX-B

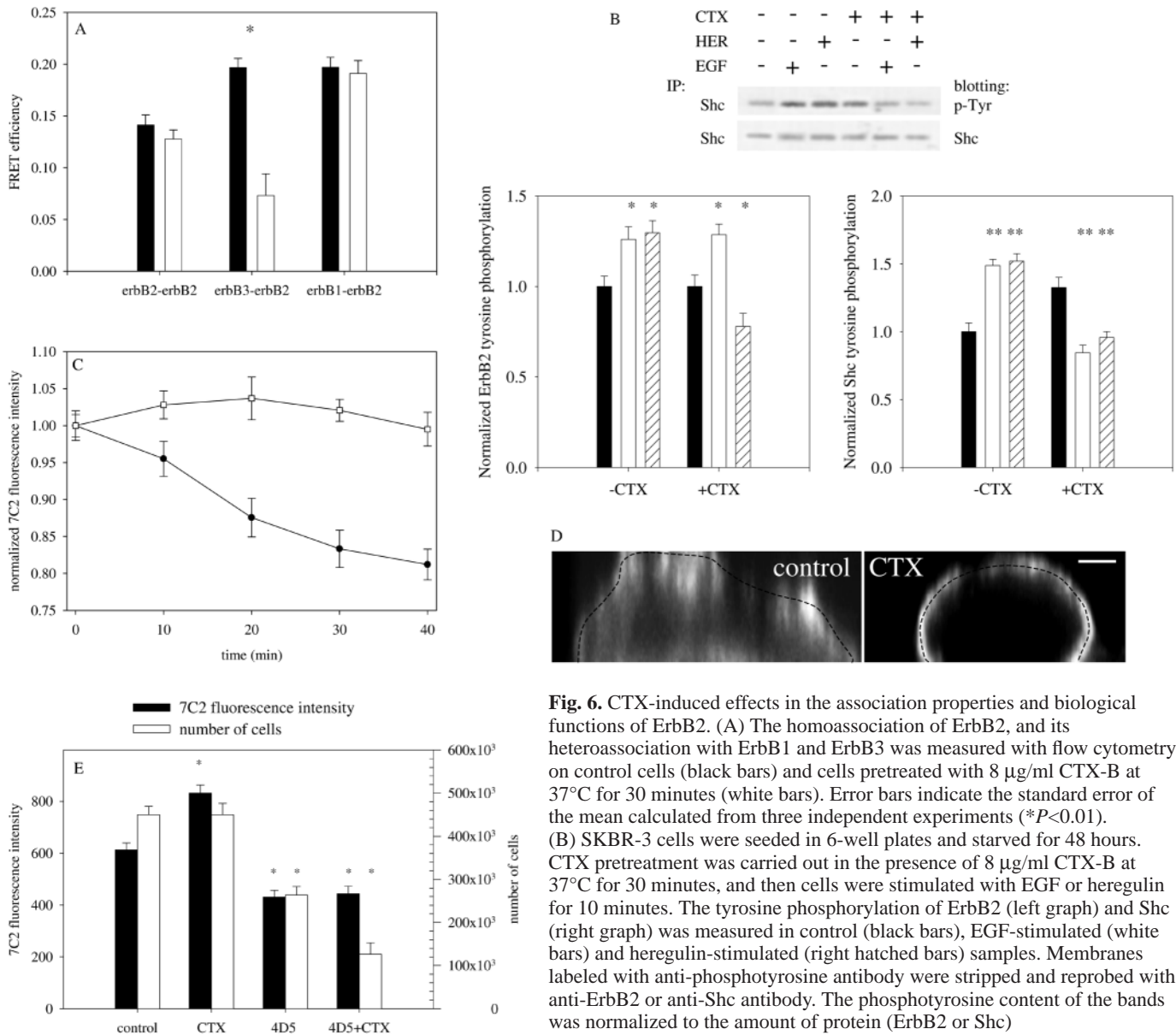
Since a heterodimer of ErbB2 and ErbB3 forms a functional

heregulin receptor, we expected a decreased effect of this growth factor on CTX-B-pretreated SKBR-3 cells. Control and CTX-B-pretreated samples were incubated in the presence of heregulin or EGF. The tyrosine phosphorylation of ErbB2 was high even in non-stimulated cells, and neither EGF, nor heregulin was able to elicit a significant increase in ErbB2 tyrosine phosphorylation ($0.05 < P < 0.1$, Fig. 6B). In CTX-B-pretreated cells, heregulin induced a marked decrease in ErbB2 tyrosine phosphorylation, indicating a shift in the balance between phosphorylation and dephosphorylation towards the latter ($P < 0.01$ for the comparison between the heregulin-induced ErbB2 tyrosine phosphorylation of CTX-B-pretreated and non-treated samples). The lack of EGF-induced response was unchanged in CTX-B-pretreated cells (Fig. 6B). In order to observe a growth factor-elicited response in SKBR-3 cells, we searched for a target downstream of ErbB2 in the signal transduction cascade. The tyrosine phosphorylation of Shc was detectable even in unstimulated cells, and treatment with either of EGF, heregulin or CTX-B induced an increase in Shc tyrosine phosphorylation. Interestingly, both EGF and heregulin induced a decrease in Shc tyrosine phosphorylation when applied to CTX-B-pretreated cells (Fig. 6B).

CTX-B significantly alters the internalization and antiproliferative effect of 4D5

The 4D5 antibody is a partial agonist of ErbB2, which after inducing tyrosine phosphorylation of ErbB2, efficiently downregulates the protein and blocks cell proliferation (Sarup et al., 1991). We investigated whether treatment of SKBR-3 cells with CTX-B alters 4D5-induced ErbB2 downregulation and the cytostatic effect of the antibody. According to flow cytometric measurements, ErbB2 was efficiently downregulated by 4D5 (Fig. 6C), a finding consistent with previous reports (Sarup et al., 1991). Furthermore, the downregulation was significantly blocked by treatment of cells with CTX-B. Three flow cytometric methods were used to monitor the downregulation of ErbB2 (described in Materials and Methods), but only one of them is shown in Fig. 6C, since results from the other approaches were the same. Flow cytometry yields statistically reliable data but requires cells in suspension. Therefore, we also used confocal microscopy to detect the internalization of fluorescently labeled 4D5 antibody and confirmed that treatment of SKBR-3 cells with CTX-B blocks the accumulation of 4D5 in the cytoplasm (Fig. 6D). We found previously that CTX-B treatment segregates lipid rafts from clusters of ErbB2 (Fig. 3D). We wanted to determine how colocalization between lipid rafts and ErbB2 clusters is influenced by co-treatment with CTX-B and 4D5. The overlap between ErbB2 clusters and lipid rafts was as low as in the case of cells treated with CTX-B alone (Fig. 3E).

The 4D5 antibody blocks the proliferation of breast tumor cells overexpressing ErbB2, and this effect is often attributed to its ability to downregulate ErbB2. Therefore, we checked whether treatment of cells with CTX-B influences the cytostatic effect of 4D5. MAb 4D5 significantly blocked the



factor-stimulated samples (* $P < 0.1$, ** $P < 0.05$). Error bars indicate the standard error of the mean calculated from three independent measurements. (C) Control (●) and CTX-pretreated (□) cells were incubated with unlabeled 4D5 antibody for 40 minutes. Samples were taken every 10 minutes, and cell surface ErbB2 was labeled with Alexa488-7C2. The fluorescence intensity of Alexa488-7C2-labeled cells was measured with flow cytometry. Error bars indicate the standard error of the mean ($n = 3$). (D) Control and CTX-pretreated SKBR-3 cells were incubated with Alexa488-4D5 antibody at 37°C for 30 minutes. Cells were imaged using confocal microscopy, and vertical slices of the cells are shown. The approximate position of the cell membrane is marked with a black dashed line (bar, 1 μm). (E) 50,000 cells were seeded in culture dishes. Control SKBR-3 cells and cells treated with 4D5, CTX-B and both with 4D5 and CTX-B were cultured for 5 days. Treatment with the antibody and CTX-B was carried out as described in Materials and Methods. At day 5 the cell surface expression of ErbB2 was measured with flow cytometry by labeling cells with Alexa488-7C2. The black bars show the mean fluorescence intensity after subtraction of autofluorescence. The number of cells is shown by the white bars. Error bars indicate the standard error of the mean (* $P < 0.05$ compared with the corresponding control, $n = 3$).

proliferation of SKBR-3 cells, and it reduced the amount of ErbB2 on the cell surface (Fig. 6E). We expected that CTX-B would hinder the antiproliferative effect of 4D5 since it prevents the internalization of ErbB2 induced by 4D5. However, 4D5 was even more efficient in blocking the proliferation of SKBR-3 cells, if they were also treated with CTX-B. CTX-B did not significantly influence the proliferation

of cells on its own but increased the amount of ErbB2 on the cell surface (Fig. 6E).

Discussion

It has been known for years that overexpression of ErbB2 significantly alters the proliferation and motility of cells

(Spencer et al., 2000), and that it is associated with poor prognosis (Slamon et al., 1987). Although many of these effects are mediated by heterodimers between ErbB2 and other ErbB proteins, ErbB2 homodimers are also present on the cell surface, particularly in cells with *c-ErbB2* gene amplification and overexpression, and these homodimers confer phenotypic effects that are likely different from that of various ErbB heterodimers (Worthylake et al., 1999; Baekstrom et al., 2000). Although much has been learned about the association properties of ErbB2, these studies failed to address the question as to how local factors influence ErbB2 association. Considering that focal activation of receptors is often observed (Brock and Jovin, 2001) we investigated the distribution of ErbB2 homoassociation in single cells.

Correlation between the association of ErbB2 and ErbB3 and their expression densities

The homoassociation of ErbB2 correlated positively with the local concentration of ErbB2, but negatively with ErbB3 local density. Consequently, membrane areas with the highest ErbB2 homoassociation displayed high and low concentrations of ErbB2 and ErbB3, respectively. The positive correlation between the local density of ErbB2 and its homoassociation probably resulted from a shift in the equilibrium between monomers and dimers of ErbB2. It has already been suggested that overexpression of ErbB2 results in constitutive homodimerization of the protein, most probably induced by a shift in the monomer-dimer equilibrium (Chamberlin and Davies, 1998; Harris et al., 1999; Worthylake et al., 1999). Our findings conform with and reinforce these previous results and point to the possible existence of a monomer-dimer equilibrium within single cells. The negative correlation between ErbB2 homoassociation and ErbB3 local density suggests that ErbB2-ErbB3 heterodimers compete with ErbB2 homodimers and therefore a high number of ErbB3 proteins can disassemble ErbB2 homodimers. A similar conclusion has already been reached based on previous work carried out on whole cell populations (Tzahar et al., 1996), but our results directly support such a competition in single cells.

Role of large-scale clustering in ErbB2 homoassociation

We have previously identified a second hierarchical level of ErbB2 association termed large-scale clustering (Nagy et al., 1999b). These large-scale clusters of ErbB2 contain $\sim 10^3$ ErbB2 proteins and their diameter is $\sim 0.5 \mu\text{m}$ in unstimulated SKBR-3 cells. We found that the extent of ErbB2 homoassociation inside clusters is not significantly different from that outside clusters. The fact that ErbB2 homoassociates even outside clusters, where the local density of the protein is low, suggests that it very avidly forms homodimers. Based on the positive correlation between the local density of ErbB2 and its homoassociation one would expect the extent of ErbB2 homoassociation to be higher inside clusters than outside. We can offer two alternative explanations. (1) The local concentration of ErbB3 is also higher inside clusters (Fig. 2B). Since ErbB3-ErbB2 dimers are preferentially formed (Tzahar et al., 1996), the higher number of ErbB3 proteins can efficiently counterbalance the effect of the increased density of ErbB2. (2) Large-scale clusters of ErbB2 colocalize with lipid

rafts, where the lipid environment decreases ErbB2 homoassociation (Figs 3, 4). Lipid rafts contain a high amount of lipids with saturated fatty acids, cholesterol and sphingolipids, and present an environment for ErbB2 that is markedly different from the bulk lipid phase. This environment might alter the association properties of ErbB2, as previously reported for another membrane protein (Vereb et al., 2000).

Involvement of lipid rafts in the association of ErbB2

According to our results ErbB2 is preferentially localized in lipid rafts. Fluorescent labeling of caveolin revealed that GM1-enriched membrane domains do not colocalize with caveolae, but crosslinking of GM1 by CTX-B induces migration of GM1 into caveolae (Fig. 5). It has been reported that GM1 appears in separate, non-caveolar membrane domains (Vyas et al., 2001), but accumulates in caveolae after crosslinking by CTX (Orlandi and Fishman, 1998; Nichols, 2002). Our results are in agreement with the above, and corroborate the existence of distinct classes of raft-like membrane domains.

Identification of a membrane protein as raft-associated is usually based on its presence in the detergent-insoluble phase of the membrane. However, this criterion is of uncertain value, because it necessitates disruption of the plasma membrane and is dependent on the nature of the detergent used (Jacobson and Dietrich, 1999). Labeling with CTX-B is accepted as a reliable raft marker (Harder et al., 1998), and application of microscopy-based approaches for the identification of raft-associated proteins has the advantage of dealing with intact plasma membranes (Jacobson and Dietrich, 1999; Kenworthy et al., 2000). The size of the domains identified by FITC-CTX-B labeling is larger than the currently accepted size of lipid rafts. However, it is acknowledged that the size and nature of lipid rafts depend upon the method of investigation (Edidin, 2001). We believe that FITC-CTX-B labeling reliably identifies lipid rafts or clusters of them.

In contrast to GPI-anchored proteins, which co-patch with CTX-B (Harder et al., 1998), lipid rafts are sequestered from ErbB2 after crosslinking with CTX-B implying a weaker interaction between raft lipids and ErbB2. Segregation of ErbB2 from lipid rafts after CTX-B treatment is not inhibited by disruption of microfilaments suggesting that cytoskeletal anchoring does not influence the raft-association of the protein. We propose that crosslinking of rafts initiates their translational diffusion in the plasma membrane, and that GPI-anchored proteins follow these motions. However, ErbB2, which has a lower lateral diffusion constant due to its transmembrane and intracellular domains, may fail to 'keep up' with the more dynamic rafts, also suggesting a less stable localization of ErbB2 in lipid rafts compared to GPI-anchored proteins.

The finding that ErbB2 is dislodged from lipid rafts and gets into the bulk lipid phase upon CTX-B treatment offered a possibility for investigating the effects of lipid environment changes on the association properties and biological function of ErbB2. Treatment of cells with CTX-B decreased the heteroassociation of ErbB2 with ErbB3, leading to inhibited tyrosine phosphorylation of Shc upon treatment with heregulin, the ligand of the ErbB2-ErbB3 heterodimer. Although the anti-Shc antibody we used recognizes both the 46 and 52 kDa forms of Shc, present in SKBR-3 cells (Le et al., 2000), we could only detect a single band. We cannot offer a rationale for this

result or for the lack of growth factor-induced tyrosine phosphorylation of ErbB2. It has already been observed by other authors that heregulin induces a hardly detectable increase in the tyrosine phosphorylation of ErbB2 (Le et al., 2000). This may be caused by the very high level of overexpression of ErbB2 in this cell line leading to self-activation of the protein (Worthylake et al., 1999). Our cell line may also be slightly different from the one used by Le and co-workers (Le et al., 2000). Neither ErbB2 homoassociation nor its heteroassociation with ErbB1 was affected by treatment with CTX-B. The fact that the EGF-induced tyrosine phosphorylation of ErbB2 was the same in control and CTX-B-pretreated cells accords nicely with this finding. However, the EGF-induced tyrosine phosphorylation of Shc was inhibited in CTX-B-pretreated cells. Previous reports suggested that Shc activation takes place inside rafts (Plyte et al., 2000), leading to the logical conclusion that ErbB2 located outside lipid rafts may not be able to activate Shc.

Internalization of ErbB2 in CTX-B-pretreated cells

Internalization of ErbB2 induced by 4D5 was significantly inhibited in cells pretreated with CTX-B. The antiproliferative effect of 4D5 is thought to be related to ErbB2 internalization followed by intracellular degradation (Sarup et al., 1991; Klapper et al., 2000; Levkowitz et al., 2000). Therefore, we expected that inhibition of ErbB2 internalization by CTX-B would be associated with decreased downregulation of ErbB2, and consequently with a decrease in the antiproliferative effect of 4D5. However, the antiproliferative effect of 4D5 was even higher in cells treated with CTX-B, suggesting that antibody-induced short-term internalization may not be a good marker for the selection of antibodies with antiproliferative effect. This proposal is in agreement with data obtained by Neve and co-workers (Neve et al., 2001), who used a single chain antibody that downregulates ErbB2 very efficiently without exerting any effect on either MAPK activity or cell proliferation. The increased cell surface expression of ErbB2 in cells treated with CTX-B alone may reflect decreased internalization of ErbB2 with a consequent shift in the equilibrium between transport of ErbB2 to and from the membrane. We do not know the reason for the increased cytostatic effect of 4D5 observed in cells treated with CTX-B. It is possible that although CTX-B slows down activation-induced internalization of ErbB2, small amounts of ErbB2 might still get internalized and degraded by a cbl-mediated pathway resulting in reduced cell proliferation (Klapper et al., 2000).

Model for the role of lipid rafts and the local density of ErbB proteins in their association

ErbB proteins form homo- and heterodimers at the molecular level and large-scale clusters in the membrane. The latter colocalize with GM1-enriched membrane domains, but are distinct from caveolae. GM1 leaves ErbB protein clusters behind upon crosslinking by CTX-B and migrates into caveolae (Fig. 7). A high local density of ErbB proteins in clusters favors their spontaneous activation, which is kept under control by the special lipid environment of rafts, that decreases ErbB2 homoassociation. A role of lipid rafts in limiting the autoactivation of the ErbB signaling system is

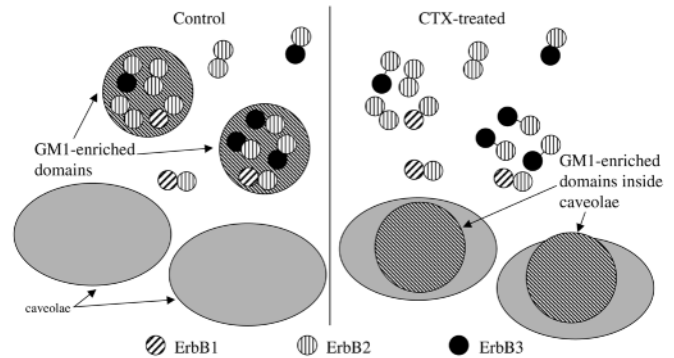


Fig. 7. Model for the association of ErbB proteins inside and outside clusters. The extent of ErbB2-ErbB2 and ErbB2-ErbB3 associations depend on the relative expression levels of the proteins: high local ErbB3 density decreases ErbB2 homoassociation. Lipid rafts, which were identified as GM1-enriched domains labeled by CTX-B in our studies, colocalize with ErbB protein clusters. Although the high local concentration of ErbB proteins inside clusters favors their spontaneous activation (e.g. the formation of highly active ErbB2 homodimers), lipid rafts keep the activation of ErbB2 under control by limiting the homodimerization of ErbB2. By contrast, ErbB proteins are maintained in a signaling competent form inside rafts (i.e. heregulin-responsive ErbB2-ErbB3 heterodimers are present), which are disassembled if ErbB proteins are removed from them. CTX-B treatment induces migration of GM1-enriched domains into caveolae and disrupts ErbB2-ErbB3, but not ErbB2-ErbB2 or ErbB2-ErbB1 dimers.

supported by the increased tyrosine phosphorylation of Shc after CTX-B treatment (Fig. 6B), which removes ErbB proteins from rafts (Fig. 3D). On the other hand, lipid rafts are also responsible for maintaining ErbB proteins in a growth factor responsive state. This is supported by the following results. (1) Neither EGF, nor heregulin is able to activate Shc, if ErbB proteins are removed from lipid rafts (Fig. 6B). (2) The formation of heregulin-responsive ErbB2-ErbB3 heterodimers and heregulin-induced ErbB2 tyrosine phosphorylation decrease, if ErbB proteins are removed from lipid rafts (Fig. 6A,B). These results parallel the suggested role of lipid rafts in T-cell-receptor-mediated signaling, where rafts are thought to be the storage sites of antigen responsive, inactive signaling components (Germain, 2001).

In summary, we have provided evidence for the role of local factors in influencing ErbB2 homoassociation. Temporal fluctuations in these factors may generate local inhomogeneities in ErbB2 homoassociation and local anomalies in signal transduction. In addition to a more thorough understanding of the complexity of the ErbB network, these results may facilitate the development of more efficient therapeutic strategies for breast cancer.

This work was supported by research grants OTKA F025210 and T037831 from the Hungarian Academy of Sciences, FKFP 0607/2000 from the Hungarian Ministry of Education, ETT 07-461/2000 from the Hungarian Ministry of Health and Welfare, FIRCA 1 R03 TW00871-01A2 and 3 P50-CA 58207 from NIH, and QRLT-1999-3126 from the European Union. P.N. was the recipient of a Fellowship from the EU Grant.

References

- Alroy, I. and Yarden, Y. (1997). The ErbB signaling network in embryogenesis and oncogenesis: signal diversification through combinatorial ligand-receptor interactions. *FEBS Lett.* **410**, 83-86.
- Anderson, R. G. and Jacobson, K. (2002). A role for lipid shells in targeting proteins to caveolae, rafts, and other lipid domains. *Science* **296**, 1821-1825.
- Baekstrom, D., Alford, D. and Taylor, P. J. (2000). Morphogenetic and proliferative responses to heregulin of mammary epithelial cells in vitro are dependent on HER2 and HER3 and differ from the responses to HER2 homodimerisation or hepatocyte growth factor. *Int. J. Oncol.* **16**, 1081-1090.
- Baulida, J. and Carpenter, G. (1997). Heregulin degradation in the absence of rapid receptor-mediated internalization. *Exp. Cell Res.* **232**, 167-172.
- Baulida, J., Kraus, M. H., Alimandi, M., di Fiore, P. P. and Carpenter, G. (1996). All ErbB receptors other than the epidermal growth factor receptor are endocytosis impaired. *J. Biol. Chem.* **271**, 5251-5257.
- Bodnár, A., Jenéi, A., Bene, L., Damjanovich, S. and Matkó, J. (1996). Modification of membrane cholesterol level affects expression and clustering of class I HLA molecules at the surface of JY human lymphoblasts. *Immunol. Lett.* **54**, 221-226.
- Brock, R. and Jovin, T. M. (2001). Heterogeneity of signal transduction at the subcellular level: microsphere-based focal EGF receptor activation and stimulation of Shc translocation. *J. Cell Sci.* **114**, 2437-2447.
- Chamberlin, S. G. and Davies, D. E. (1998). A unified model of c-erbB receptor homo- and heterodimerisation. *Biochim. Biophys. Acta* **1384**, 223-232.
- Cobleigh, M. A., Vogel, C. L., Tripathy, D., Robert, N. J., Scholl, S., Fehrenbacher, L., Wolter, J. M., Paton, V., Shak, S., Lieberman, G. et al. (1999). Multinational study of the efficacy and safety of humanized anti-HER2 monoclonal antibody in women who have HER2-overexpressing metastatic breast cancer that has progressed after chemotherapy for metastatic disease. *J. Clin. Oncol.* **17**, 2639-2648.
- Demandolx, D. and Davoust, J. (1997). Multiparameter image cytometry: from confocal micrographs to subcellular fluorograms. *Bioimaging* **5**, 159-169.
- Edidin, M. (2001). Shrinking patches and slippery rafts: scales of domains in the plasma membrane. *Trends Cell Biol.* **11**, 492-496.
- Furuchi, T. and Anderson, R. G. (1998). Cholesterol depletion of caveolae causes hyperactivation of extracellular signal-related kinase (ERK). *J. Biol. Chem.* **273**, 21099-21104.
- Germain, R. N. (2001). The T cell receptor for antigen: signaling and ligand discrimination. *J. Biol. Chem.* **276**, 35223-35226.
- Glasbey, C. A. and Horgan, G. W. (1995). Mathematical morphology. In *Image Analysis for the Biological Sciences* (ed. C. A. Glasbey and G. W. Horgan), pp. 125-152. John Wiley & Sons.
- Graus Porta, D., Beerli, R. R., Daly, J. M. and Hynes, N. E. (1997). ErbB-2, the preferred heterodimerization partner of all ErbB receptors, is a mediator of lateral signaling. *EMBO J.* **16**, 1647-1655.
- Harder, T. and Simons, K. (1997). Caveolae, DIGs, and the dynamics of sphingolipid-cholesterol microdomains. *Curr. Opin. Cell Biol.* **9**, 534-542.
- Harder, T., Scheffele, P., Verkade, P. and Simons, K. (1998). Lipid domain structure of the plasma membrane revealed by patching of membrane components. *J. Cell Biol.* **141**, 929-942.
- Harris, R. A., Eichholtz, T. J., Hiles, I. D., Page, M. J. and O'Hare, M. J. (1999). New model of ErbB-2 over-expression in human mammary luminal epithelial cells. *Int. J. Cancer* **80**, 477-484.
- Hwang, J., Gheber, L. A., Margolis, L. and Edidin, M. (1998). Domains in cell plasma membranes investigated by near-field scanning optical microscopy. *Biophys. J.* **74**, 2184-2190.
- Ilangumaran, S., Arni, S., van Echten-Deckert, G., Borisch, B. and Hoessli, D. C. (1999). Microdomain-dependent regulation of Lck and Fyn protein-tyrosine kinases in T lymphocyte plasma membranes. *Mol. Biol. Cell* **10**, 891-905.
- Jacobson, K. and Dietrich, C. (1999). Looking at lipid rafts? *Trends. Cell Biol.* **9**, 87-91.
- Janes, P. W., Ley, S. C. and Magee, A. I. (1999). Aggregation of lipid rafts accompanies signaling via the T cell antigen receptor. *J. Cell Biol.* **147**, 447-461.
- Jovin, T. M. and Arndt Jovin, D. J. (1989). FRET microscopy: Digital imaging of fluorescence resonance energy transfer. Application in cell biology. In *Cell Structure and Function by Microspectrofluorometry* (ed. E. Kohen and J. G. Hirschberg), pp. 99-117. San Diego, CA: Academic Press.
- Karunakaran, D., Tzahar, E., Beerli, R. R., Chen, X., Graus Porta, D., Ratzkin, B. J., Seger, R., Hynes, N. E. and Yarden, Y. (1996). ErbB-2 is a common auxiliary subunit of NDF and EGF receptors: implications for breast cancer. *EMBO J.* **15**, 254-264.
- Kenworthy, A. K., Petranova, N. and Edidin, M. (2000). High-resolution FRET microscopy of cholera toxin B-subunit and GPI-anchored proteins in cell plasma membranes. *Mol. Biol. Cell* **11**, 1645-1655.
- Klapper, L. N., Waterman, H., Sela, M. and Yarden, Y. (2000). Tumor-inhibitory antibodies to HER-2/ErbB-2 may act by recruiting c-Cbl and enhancing ubiquitination of HER-2. *Cancer Res.* **60**, 3384-3388.
- Kurzchalia, T. V. and Parton, R. G. (1999). Membrane microdomains and caveolae. *Curr. Opin. Cell Biol.* **11**, 424-431.
- Le, X. F., Vadlamudi, R., McWatters, A., Bae, D. S., Mills, G. B., Kumar, R. and Bast, R. C., Jr (2000). Differential signaling by an anti-p185(HER2) antibody and heregulin. *Cancer Res.* **60**, 3522-3531.
- Levkowitz, G., Klapper, L. N., Tzahar, E., Freywald, A., Sela, M. and Yarden, Y. (1996). Coupling of the c-Cbl protooncogene product to ErbB-1/EGF-receptor but not to other ErbB proteins. *Oncogene* **12**, 1117-1125.
- Levkowitz, G., Oved, S., Klapper, L. N., Warari, D., Lavi, S., Sela, M. and Yarden, Y. (2000). c-Cbl is a suppressor of the neu oncogene. *J. Biol. Chem.* **275**, 35532-35539.
- Matkó, J., Bodnár, A., Vereb, G., Bene, L., Vámosi, G., Szentesi, G., Szöllösi, J., Gáspár, R., Jr, Horejsi, V., Waldmann, T. A. et al. (2002). GPI-microdomains (membrane rafts) and signaling of the multi-chain interleukin-2 receptor in human lymphoma/leukemia T cell lines. *Eur. J. Biochem.* **269**, 1199-1208.
- Mineo, C., Gill, G. N. and Anderson, R. G. (1999). Regulated migration of epidermal growth factor receptor from caveolae. *J. Biol. Chem.* **274**, 30636-30643.
- Nagy, P., Bene, L., Balázs, M., Hyun, W. C., Lockett, S. J., Chiang, N. Y., Waldman, F. M., Feuerstein, B. G., Damjanovich, S. and Szöllösi, J. (1998). EGF-induced redistribution of erbB2 on breast tumor cells: Flow and image cytometric energy transfer measurements. *Cytometry* **32**, 120-131.
- Nagy, P., Jenéi, A., Damjanovich, S., Jovin, T. M. and Szöllösi, J. (1999a). Complexity of signal transduction mediated by erbB2: clues to the potential of receptor-targeted cancer therapy. *Pathol. Oncol. Res.* **5**, 255-271.
- Nagy, P., Jenéi, A., Kirsch, A. K., Szöllösi, J., Damjanovich, S. and Jovin, T. M. (1999b). Activation-dependent clustering of the erbB2 receptor tyrosine kinase detected by scanning near-field optical microscopy. *J. Cell Sci.* **112**, 1733-1741.
- Neve, R. M., Nielsen, U. B., Kirpotin, D., Poul, M. A., Marks, J. D. and Benz, C. C. (2001). Biological effects of anti-ErbB2 single chain antibodies selected for internalizing function. *Biochem. Biophys. Res. Commun.* **280**, 274-279.
- Nichols, B. J. (2002). A distinct class of endosome mediates clathrin-independent endocytosis to the Golgi complex. *Nat. Cell Biol.* **4**, 374-378.
- Orlandi, P. A. and Fishman, P. H. (1998). Filipin-dependent inhibition of cholera toxin: evidence for toxin internalization and activation through caveolae-like domains. *J. Cell Biol.* **141**, 905-915.
- Park, J. W., Tripathy, D., Campbell, M. J. and Esserman, L. J. (2000). Biological therapy of breast cancer. *Biodrugs* **14**, 221-245.
- Pinkas Kramarski, R., Shelly, M., Glathe, S., Ratzkin, B. J. and Yarden, Y. (1996). Neu differentiation factor/neuregulin isoforms activate distinct receptor combinations. *J. Biol. Chem.* **271**, 19029-19032.
- Plyte, S., Majolini, M. B., Pacini, S., Scarpini, F., Bianchini, C., Lanfrancone, L., Pelicci, P. and Baldari, C. T. (2000). Constitutive activation of the Ras/MAP kinase pathway and enhanced TCR signaling by targeting the Shc adaptor to membrane rafts. *Oncogene* **19**, 1529-1537.
- Pralle, A., Keller, P., Florin, E. L., Simons, K. and Horber, J. K. (2000). Sphingolipid-cholesterol rafts diffuse as small entities in the plasma membrane of mammalian cells. *J. Cell Biol.* **148**, 997-1008.
- Sarup, J. C., Johnson, R. M., King, K. L., Fendly, B. M., Lipari, M. T., Napier, M. A., Ullrich, A. and Shepard, H. M. (1991). Characterization of an anti-p185HER2 monoclonal antibody that stimulates receptor function and inhibits tumor cell growth. *Growth Regul.* **1**, 72-82.
- Simons, K. and Ikonen, E. (1997). Functional rafts in cell membranes. *Nature* **387**, 569-572.
- Slamon, D. J., Clark, G. M., Wong, S. G., Levin, W. J., Ullrich, A. and McGuire, W. L. (1987). Human breast cancer: correlation of relapse and survival with amplification of the HER-2/neu oncogene. *Science* **235**, 177-182.
- Slamon, D. J., Leyland-Jones, B., Shak, S., Fuchs, H., Paton, V., Bajamonde, A., Fleming, T., Eiermann, W., Wolter, J., Pegram, M. et al. (2001). Use of chemotherapy plus a monoclonal antibody against HER2

- for metastatic breast cancer that overexpresses HER2. *New Engl. J. Med.* **344**, 783-792.
- Sliwkowski, M. X., Lofgren, J. A., Lewis, G. D., Hotaling, T. E., Fendly, B. M. and Fox, J. A.** (1999). Nonclinical studies addressing the mechanism of action of trastuzumab (Herceptin). *Semin. Oncol.* **26**, 60-70.
- Spencer, K. S. R., Graus, P., Leng, J., Hynes, N. E. and Klemke, R. L.** (2000). ErbB2 is necessary for induction of carcinoma cell invasion by ErbB family receptor tyrosine kinases. *J. Cell Biol.* **148**, 385-397.
- Szöllösi, J., Trón, L., Damjanovich, S., Helliwell, S. H., Arndt Jovin, D. and Jovin, T. M.** (1984). Fluorescence energy transfer measurements on cell surfaces: a critical comparison of steady-state fluorimetric and flow cytometric methods. *Cytometry* **5**, 210-216.
- Tzahar, E., Waterman, H., Chen, X., Levkowitz, G., Karunagaran, D., Lavi, S., Ratzkin, B. J. and Yarden, Y.** (1996). A hierarchical network of interreceptor interactions determines signal transduction by Neu differentiation factor/neuregulin and epidermal growth factor. *Mol. Cell. Biol.* **16**, 5276-5287.
- Vereb, G., Matkó, J., Vamosi, G., Ibrahim, S. M., Magyar, E., Varga, S., Szöllösi, J., Jenei, A., Gáspár, R., Jr, Waldmann, T. A. et al.** (2000). Cholesterol-dependent clustering of IL-2Ralpha and its colocalization with HLA and CD48 on T lymphoma cells suggest their functional association with lipid rafts. *Proc. Natl. Acad. Sci. USA* **97**, 6013-6018.
- Vyas, K. A., Patel, H. V., Vyas, A. A. and Schnaar, R. L.** (2001). Segregation of gangliosides GM1 and GD3 on cell membranes, isolated membrane rafts, and defined supported lipid monolayers. *Biol. Chem.* **382**, 241-250.
- Worthylake, R., Opresko, L. K. and Wiley, H. S.** (1999). ErbB-2 amplification inhibits down-regulation and induces constitutive activation of both erbB-2 and epidermal growth factor receptors. *J. Biol. Chem.* **274**, 8865-8874.
- Wouters, F. S., Bastiaens, P. I., Wirtz, K. W. and Jovin, T. M.** (1998). FRET microscopy demonstrates molecular association of non-specific lipid transfer protein (nsL-TP) with fatty acid oxidation enzymes in peroxisomes. *EMBO J.* **17**, 7179-7189.
- Yarden, Y. and Sliwkowski, M. X.** (2001). Untangling the ErbB signalling network. *Nat. Rev. Mol. Cell. Biol.* **2**, 127-137.